

On the design of an acoustical test fixture for assessing the objective occlusion effect

Olivier Doutres^{a,*}, Yu Luan^a, Marc-Olivier Cyr-Desroches^a, Kévin Carillo^a, Robin Richert^b, Franck Sgard^c

^a Department of Mechanical Engineering, École de Technologie Supérieure (ÉTS), Canada

^b École Nationale Supérieure d'Ingénieurs du Mans (ENSIM), Le Mans Université, Le Mans, France

^c Institut de recherche Robert-Sauvé en santé et en sécurité du travail (IRSST), Canada

ARTICLE INFO

Keywords:

Occlusion effect

Earplug

Acoustical test fixture

Bone conduction

ABSTRACT

Earplugs are widely used to prevent noise induced hearing loss. However, the discomforts they induce negatively impact their effectiveness by influencing their consistent and correct use. The occlusion effect discomfort is related to an increased perception of the bone-conducted part of physiological sounds (e.g., one's own voice, breathing and chewing) when one's ear canal is occluded. The discomfort experienced could be objectively estimated by calculating the objective occlusion effect, which is the difference between the tympanic sound pressure levels in the occluded and open ear canals when exposed to the same stimulation of a bone transducer. To avoid direct measurements on human participants, this work proposes an acoustical test fixture (ATF) for quantifying the objective occlusion effect. The proposed ATF employs an anatomically realistic truncated ear, incorporating soft tissues, cartilage, and bone components to replicate the outer ear bone conduction path crucial for occlusion effect assessments. It is shown that the proposed ATF can reproduce key effects observed in objective OE measurements on human participants: (i) significant OE at low frequencies, diminishing with increasing frequency, (ii) reduction of OE with greater insertion depths, and (iii) distinctions among various earplug types, particularly noticeable at deeper insertions compared to shallow ones. The proposed ATF can therefore be used to design in-ear devices with a reduced occlusion effect, leading to an improved experience for many users of hearing protectors, hearing aids, and earbuds. Additionally, a computationally efficient Finite Element Method-based virtual tester for the ATF is developed and validated. This virtual tester is employed to deepen the comprehension of the physical phenomena that underlie the observed vibroacoustic behavior of the proposed ATF. It also opens avenues for future research aimed at re-evaluating ATF design parameters and enhancing OE assessment.

1. Introduction

Hearing protection devices, such as earplugs are commonly used as the last resort to protect workers exposed to hazardous noise. However, the wearing of earplugs is usually accompanied with discomfort issues, which can prevent them from being properly worn and thus reduce their efficiency in the workplace [1]. The occlusion effect constitutes one of these issues. It corresponds to an increased perception of the bone-conducted part of physiological sounds (e.g., one's own voice, breathing and chewing) when one's ear canal is occluded [2]. This phenomenon is found to be typically significant at frequencies lower than 1 – 2 kHz [3,4], and involves all the bone conduction paths (i.e., outer, middle

and inner ears). As the bone conduction hearing in an occluded ear is particularly dominated by the outer ear path at low frequencies [5], the experienced occlusion effect could be estimated objectively by calculating the difference between the tympanic sound pressure levels in the occluded and open ear canals when one's head is subjected to the same stimulation of a bone transducer [4,6,7]. This indicator is commonly referred to as the objective OE and simply OE in this paper for the sake of conciseness.

Instead of direct measurements on human participants, an acoustical test fixture (ATF) could be a useful tool for quantifying the OE induced by earplugs (or any in-ear device such as hearing aids or earbuds), studying the associated vibroacoustic behaviors, and designing more

* Corresponding author.

E-mail address: olivier.doutres@etsmtl.ca (O. Doutres).

<https://doi.org/10.1016/j.apacoust.2024.110295>

Received 16 December 2023; Received in revised form 26 July 2024; Accepted 13 September 2024

Available online 20 September 2024

0003-682X/© 2024 The Author(s). Published by Elsevier Ltd. This is an open access article under the CC BY-NC-ND license (<http://creativecommons.org/licenses/by-nc-nd/4.0/>).

comfortable earplugs with a reduced OE [8,9]. Indeed, the use of ATF allows for quick, straightforward and repeatable measurements as required in some quality assurance or design applications. Additionally, they can serve as standardized experimental testing. Existing ATFs as specified in the ANSI S12.42 standard [10] have been designed to assess the insertion loss of hearing protection devices (earplugs and earmuffs) in continuous or impulsive noises. While a flesh simulation that includes a skin layer covering the inner walls of the ear canal and the pinna is considered, the bone conduction through the head and outer ear is not adequately integrated into their design, making them *a priori* unsuitable for OE measurements.

In this pursuit, several studies in the literature have endeavored to create ATFs that are anatomically more realistic, incorporating soft tissues, cartilage, and bone components and specifically designed for investigating the OE induced by earplugs [11–19]. These studies can be categorized into two main groups based on the geometry considered: full head [11–13] or truncated outer ears [14–19]. Throughout the manuscript, it is important to note that the term ATF encompasses the structure (head or truncated ear) serving as the housing for the earplug, its fixation apparatus, the instrumentation and the excitation system. The aforementioned studies also generally propose virtual testers, such as numerical models based on the finite element (FE) method. These models contribute to a more profound comprehension of the underlying physical phenomena governing OE and allow for a convenient reassessment of ATF design parameters to enhance OE assessments. As importantly, these virtual testers could ultimately be used for designing more comfortable earplugs. However, to be used for that purposes, virtual testers should be first validated from their corresponding ATFs. Such task is challenging considering the difficulty in matching the geometry, the loading and the boundary conditions of both the numerical model and the experimental setup.

Studies incorporating a full head system more effectively capture bone-conducted sound across the entire head, eliminating the truncation of tissues around the ear canal. This, in turn, facilitates the definition and application of loading and boundary conditions on the ATF and its associated virtual tester. However, the use of such a large model can be time consuming, and the associated physical replica is more expensive and complex to manufacture.

Truncated outer ears, which are the object of this work, are smaller systems more suitable for use as tabletop measurement benches. The associated numerical models are also faster to solve and hence allow the analysis of a large number of variables. They have thus been widely used in the past to better understand the fundamental physical phenomena underlying the OE [7,15,18,19]. Usually, the set of mechanical boundary conditions and loading applied to truncated ears was tailored to either achieve simulation results that align with experimental data of the OE [14,15,18], replicate a plausible vibration pattern of the ear canal wall [7,19], or was kept as simple as possible to ensure ease of experimental reproducibility [20]. Brummund and his colleagues were the first to conduct research on truncated outer ears for OE assessment [14,21]. They proposed a 2D axisymmetric truncated artificial ear with a cylindrical-shaped ear canal in order to validate experimentally the OE simulated by a FE model. This artificial ear suffered from a few limitations. First, it had an oversized cartilage part, which was not representative of a real human ear. Second, the test bench used for experimental validation provided an excitation in the shear direction rather than in the radial direction to the ear canal walls, which was different from the loading condition defined in the model. Furthermore, the loading was directly applied to the bone structure which differs from the tests conducted on human participants, where a bone transducer is directly placed on the soft tissues. Third, due to limited time and resources of the study, this artificial ear had not been fully tested and validated [14]. More recently, an ATF and its associated virtual tester based on a realistic 3D truncated artificial ear has been developed for OE prediction, whose geometry was reconstructed from medical images of a real human ear [17,20,22]. In contrast to the previous ATF, this artificial ear not

only differentiated cartilage from soft tissues such as skin, fat, and muscles but was also integrated into a bony structure, encompassing the complete pinna. The loading condition remained unrealistic as it was applied to the bony portion of the ear. Significant disparities were observed between the simulated and measured sound pressure levels in both the open and occluded ear canals, prompting various hypotheses to explain these inconsistencies. For instance, challenges were encountered in accurately modeling the interaction between the earplug and soft tissues, as well as in characterizing the mechanical properties of the materials involved. Recently, a parallelepipedic outer ear has been employed to assess the OE of various earplugs and, more notably, validate novel concepts of *meta*-earplugs aimed at mitigating this effect [8,9]. Bone-conducted stimulation was applied using the shaker of a quasi-static mechanical analyzer (QMA), targeting the soft tissues this time. The artificial ear experienced a static compression between the shaker plate and a fixed rigid element of the QMA, which dictated the selection of a parallelepipedic geometry for the artificial ear. Even though this ATF has proven its ability to quantify the OE of some earplugs, the validation of the associated numerical model was not successful [23]. The significant disparities between measurements and calculations were hypothesized to stem from: (i) fabrication defects in the artificial ear prototype, (ii) material properties not adequately characterized and (iii) vibrations in the test bench, factors not accounted for in the model. To sum up, the literature review shows that there is currently no ATF based on a truncated ear systematically used to quantify OE induced by earplugs. Moreover, OE virtual testers based on truncated ears have never been validated against measurements performed on their corresponding ATFs. As a result, virtual testers based on truncated outer ears are generally considered valid when their deterministic simulation of OE fits into the measurement variability observed in a group of human subjects (considering the same earplug type and insertion depth in both modeling and measurements).

This paper is an extension of the work of Luan et al. [23] on the parallelepipedic outer ear-based ATF. The goals are twofold: (i) assess the ability of the proposed ATF to reproduce key effects observed in objective OE measurements on human participants and (ii) validate the associated virtual tester, a step not previously undertaken. The aforementioned key effects intended to be replicated by the ATF include (i) significant OE at low frequencies, diminishing with increasing frequency, (ii) reduction of OE with greater insertion depths, and (iii) distinctions among various earplug types, particularly noticeable at deeper insertions compared to shallow ones. Both goals are achieved by carefully selecting the ATF characteristics (e.g., loading, boundary conditions).

The paper is organized as follows. Section 2 recalls the design and fabrication of the truncated artificial ear of the proposed ATF for measuring the OE. Section 3 introduces the experimental setups and the earplugs tested. The ATF is detailed, along with methods employed for characterizing the mechanical properties of the soft tissue material in the artificial ear. Sections 4 and 5 respectively present the virtual tester based on the FE method and the indicators of interest. Section 6 is dedicated to presenting and discussing results. Following the mechanical characterization details, the experimental validation of the virtual tester is accomplished by comparing simulated OE with experimental data from the ATF. The vibroacoustic behavior of the ATF is explored numerically in both open and occluded configurations to further investigate the assessed OE. Subsequently, further measurements are undertaken to evaluate the realism of the ATF in comparison to measurements carried out on human participants, as well as its ability to accurately depict the effects of different earplug types and insertion depths on OE.

2. Design and fabrication of the artificial ear

As mentioned in the introduction, the design of an ATF for OE assessments based on a truncated artificial ear should avoid the problems

identified from previous studies in the literature while keeping most of their advantages. From a numerical point of view, it needs to be simple in geometry in order to reduce computational costs for simulations but still to be able to capture the main vibroacoustic behaviors associated with the OE. From an experimental viewpoint, the OE should be measured with available resources in a laboratory on the designed artificial ear, using similar loading and boundary conditions as in numerical models.

The designed artificial ear is shown in Fig. 1(a) in symmetric view, which includes the earcanal surrounding tissues essential for the bone conduction through the outer ear, i.e., bone, cartilage and soft tissues [16,23]. The proportion of their volumes is kept unchanged relative to the realistic 3D artificial ear proposed by Benacchio et al. [22], whose geometry was reconstructed from a real human ear. Particularly, a parallelepiped shape is adopted for this artificial ear to facilitate the experimental manipulation on the ATF (see section 3.1 for the details on the proposed ATF). This straightforward geometry results in a virtual tester with numerically efficient simulations at a low computational cost. A simple cylindrical earcanal with a constant cross-section is chosen here, following the approach of standardized ATFs dedicated to sound attenuation measurements [10]. This selection aims to assess the acoustic behavior of the coupled “earcanal/earplug” system, generally representative of humans. The advantage of this choice lies in its ease of accounting for the coupling between the earplug and earcanal walls in numerical simulations, facilitating model validation. However, similar to standardized ATFs, a drawback is evident as it hinders the analysis of inter-variability effects resulting from earplug insertions into ears of various shapes. Therefore, for a comprehensive study involving ears of different shapes representing specific populations, a broader scope would be necessary [24], however exceeding the objectives of this work. The earcanal in the proposed outer ear includes both cartilaginous and bony parts. The transition between the two occurs approximately at the midpoint of the earcanal, consistent with information found in the literature [6]. The proposed artificial ear does not consider the middle and inner ears, as the outer ear pathway predominantly influences bone conduction at low frequencies when the earcanal is occluded [5]. Furthermore, our focus is solely on the objective OE which is defined as the difference of sound pressure levels at the eardrum in the occluded and open earcanals. While existing models typically account for the middle and inner ears using an acoustic impedance at the eardrum position [17], those components are not considered here to simplify the model validation process and the ATF. Therefore, a bony part closes the earcanal (i.e., at the eardrum position) but is perforated to accommodate the sensing device for sound pressure measurements (see section 3.1).

After finalizing the design of the artificial ear, True Phantom Solutions (Windsor, Canada) fabricated a corresponding prototype. Epoxy-based composite material and urethane-based soft resins of various hardnesses were employed to replicate the behaviors of bone, cartilage,

and soft tissues (see Fig. 1(b)).

3. Experimental setups and materials

3.1. ATF

The ATF shown in Fig. 2 is mainly composed of (i) the truncated artificial ear (see section 2), (ii) three sensors (i.e., a miniature microphone and two accelerometers) and (iii) a test bench to apply the bone-conduction excitation and the mechanical boundary conditions. The test bench is a commercial QMA (Mecanum, Canada) available at the laboratory (see Fig. 3(a)). This test bench uses an electrodynamic shaker to generate the stimulation and allows to set different boundary conditions at the top “bony” side of the ear. In the baseline configuration of the proposed ATF, the top of the artificial ear is let free so that the ear is expected to behave as a simple mass-spring resonator at low frequencies. However, the QMA test bench also allows to bond the top bony part (as described in more details in the Appendix B) thanks to a mechanical system made of a rigid plate attached to a worm screw.

On the “soft side” of the artificial ear (i.e., bottom of the ear covered by soft tissues), a perpendicular transfer of vibratory energy from the shaker to the ear is achieved using an aluminum plate, denoted as the “excitation plate.” The choice of using a plate is justified by the necessity to control the noise produced by the excitation system and replicate it accurately within the virtual tester (see section 4). This assumes that the ATF-generated noise is primarily dominated by the radiation of the excitation plate and the surfaces of the artificial ear. Double-sided tape is used to ensure the contact between the plate and the ear (see Fig. 2(a)). The electrodynamic shaker is fed with white noise using an audio signal generator (MR2, NTI Audio, Liechtenstein). The input signal is adjusted in order to obtain a sound pressure level of at least 10 dB higher than the background noise in the open ear over the frequency range of interest between 100 Hz and 1250 Hz. An accelerometer (from a mechanical impedance sensor, 288D01, PCB Piezotronics, USA) is attached between the shaker and the excitation plate for measuring the acceleration at its center. Another accelerometer (322A41, Dytran Instruments Inc., USA) measures the acceleration at the top bony side of the ear. A miniature microphone (Knowles®, USA) housed in its casing is carefully inserted into a probe-tube, which traverses a small aperture in the bony section, and is flush-mounted at the end of the earcanal to measure the sound pressure at the “eardrum position”. It was chosen to place the microphone in a tube rather than directly in the bony part to prevent it from vibrating and contaminating the generated acoustic pressure signal. Mounting putty is placed carefully at the back of the ear around the plastic tube in order to avoid potential sound leaks (see Fig. 2(b)). The probe-tube microphone is calibrated by positioning its opening adjacent to a calibrated ¼ in. reference microphone (multi-field microphone type 4961, Brüel & Kjaer, Denmark) within an audiometric booth. An 85 dB

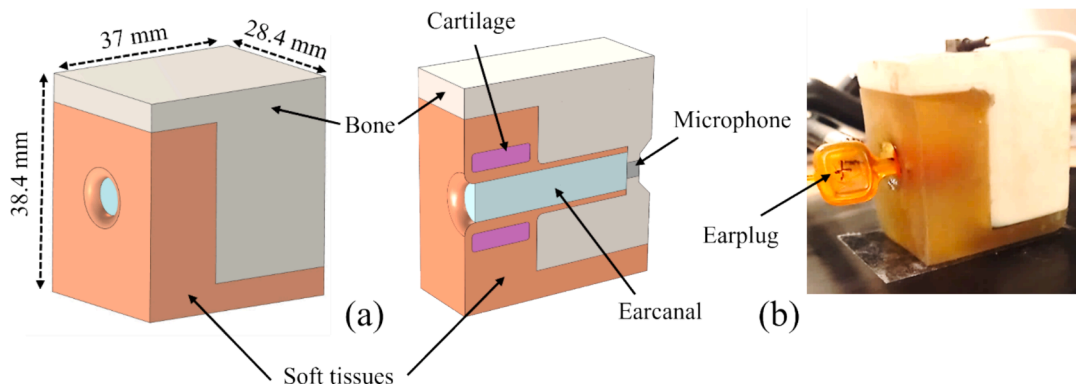


Fig. 1. (a) Designed parallelepipedic artificial ear (solid geometry and cut through the mid-plane); (b) Fabricated artificial ear occluded by a commercial earplug (“Push-to-fit foam pod 3” see Table 1).

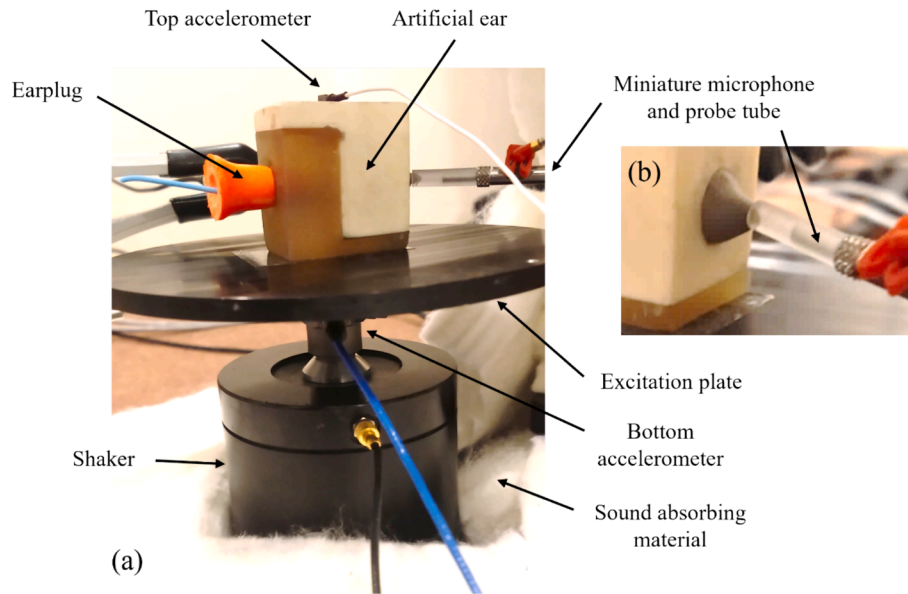


Fig. 2. (a) ATF based on a parallelepipedic artificial ear prototype. The artificial ear is occluded by a roll-down foam earplug. (b) Rear view of the artificial ear to show the installation of the probe-tube microphone.

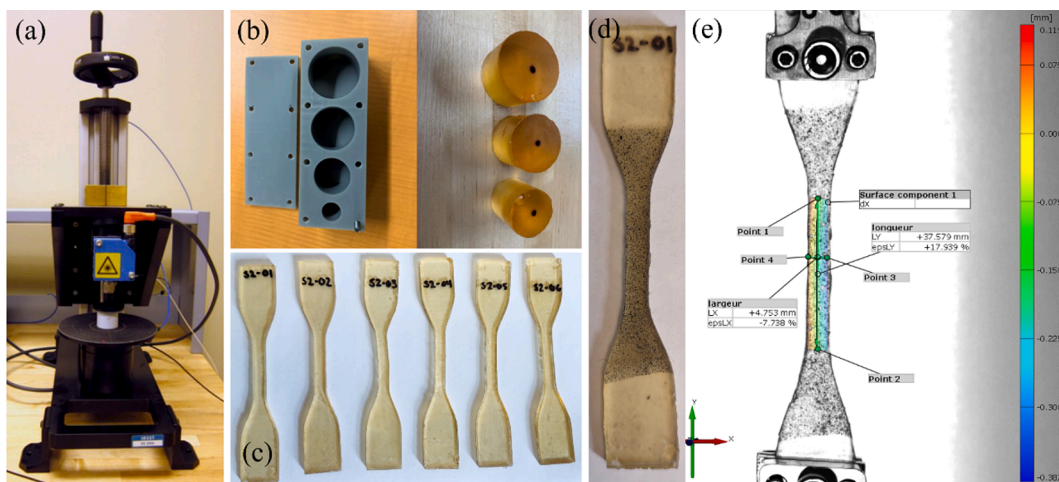


Fig. 3. Characterization of the soft tissue material: (a) Quasistatic mechanical analyser (QMA); (b) cylindrical molds (left) and samples (right) for QMA testing, (c) dumbbell-shaped samples for tensile tests, (d) stochastic pattern for strain field analysis, (e) strain field analysis for Poisson coefficient assessment.

(A) uncorrelated Gaussian white noise with four speakers is then generated, allowing the calculation of a frequency-dependent calibration factor. Finally, for OE measurements, the ATF is placed in the same audiometric booth with a low-level background noise and sound absorbing walls. Sound absorbing materials are also placed below the excitation plate as well as on the structure of the QMA. This selection is justified by the need for measurement conditions during the model validation phase to closely match those of the FE model, particularly critical for the open ear canal configuration. The indicators of interest (including the OE) obtained using the proposed ATF are presented in Section 5.

3.2. Mechanical characterization of the soft tissue material

Considering the difficulty in assessing the mechanical properties of the soft tissue material, the following three different techniques were carried out: (1) compression tests on cylindrical specimens, (2) tensile test on dumbbell-shaped samples and (3) an inverse technique based on the transmissibility measured on the proposed ATF.

3.2.1. Compression tests

Mechanical characterization based on the compression of samples was carried out following the standard ISO 18437–5:2011 [25] and using a commercial QMA (Mecanum, Canada) (see Fig. 3(a)). The method is based on the compression of cylindrical samples of different shape factors (see Fig. 3(b)) with bonded boundary conditions at both ends. The measurement of the samples' mechanical impedance and FEM calculations of those conditions as a function of Poisson's ratio allows to determine the Young's Modulus, the loss factor and the Poisson's ratio of the material. All samples are 25 mm-thick and the diameters are 25, 30 and 35 mm. The static compression rate applied to the samples is of 0.8 %. The tests were performed at laboratory air conditions (21 °C).

3.2.2. Tensile tests

Tensile tests were applied to dumbbell-shaped samples according to the standard ASTM D412 [26] (see Fig. 3(c)). Using a Bose Electroforce 3220-AT machine equipped with a load cell of 22 N, the samples were stretched 5 times to 10 mm in order to precondition the samples and avoid the Mullin effect [27]. Tests were performed with 1 mm/s strain

rate and at room temperature (~20 °C). The Young’s modulus was determined from the stress–strain curve of the 5th stretching cycle. A linear trend curve was generated by considering the data from 2 % deformation up to the maximum stretch of 10 mm. The slope of this trend curve represents the Young’s modulus of the sample. The Poisson’s ratio of the samples were calculated following the standard procedure ASTM E132-17 [28] from axial and transverse strains captured with an optical system (Aramis 5 M, Gom professional 2019, see Fig. 3(e)) and plotted as a function of force. The Poisson’s ratio was determined by dividing the slope of the transverse axis curve by that of the axial axis. For the analysis of the strain field of the samples, a stochastic pattern must be painted on the region of interest of the samples, namely the narrow central section (see Fig. 3(d) and (e)).

3.2.3. Transmissibility tests

As mentioned earlier, the acceleration transmissibility between the top and bottom sides of the truncated ear was measured. The properties of the soft tissue material used in the virtual tester presented in the following (see section 4) were then calibrated using the transmissibility measurements at low frequencies. This indirect method enables the determination of Young’s Modulus, the loss factor, and the Poisson’s ratio for the soft tissue exclusively and solely at low frequencies (frequency $f < 300$ Hz) where two structural resonances (one of them being the pumping motion resonance) of the ear dominate the truncated ear vibratory behavior (see section 6.1).

3.3. Earplugs

The earplugs examined in this study are listed in Table 1, along with their corresponding insertion depths.

The occlusion device used to validate the virtual tester is a custom-molded silicone earplug, which is shallowly inserted into the earcanal. Its total length is 14 mm, and the length of the inserted part is about 6 mm. The diameter of the earplug is slightly larger than that of the earcanal in order to ensure a good sealing condition.

The evaluation of the proposed ATF is further carried out using multiple types of earplugs. Five of them are commercial disposable and reusable earplugs: two earplugs belong to the “roll-down-foam” family, one is a multi-flange from the “pre-molded” earplug family, and two are from the “push-to-fit foam” earplug family. The earplugs used in this study were purchased from various manufacturers, and the references of these manufacturers are furnished in Table 1 to enhance the reproducibility of the study. Subsequently, throughout the remainder of the paper, the earplugs are denoted by their respective classifications.

Additionally, two custom-made occlusion devices belonging to the push-to-fit foam earplug category are included. Both devices utilize



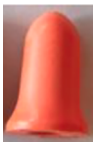





Comply isolation ear-tips (Comply, St. Paul, USA) for fitting into the earcanal. The first device, referred to as “Push-to-fit foam pod 1”, is a custom-made earpiece previously employed by the research team to explore various measurement methods of the objective OE on human participants [29]. The incorporation of this occlusion device enables the assessment of the fidelity of the proposed ATF by comparing its outcomes with OE measurements conducted on human participants (as referenced in [29]). This occlusion device provides control over the insertion depth, ensuring consistent conditions between the ATF and participant conditions. The measurements extracted from [29] involve the use of mastication as an excitation source, and the computation of the standard occlusion effect (i.e., the difference between occluded and open earcanal sound pressure levels). It is noteworthy that [29] establishes that mastication as an excitation source yields OE outcomes comparable to those achieved through a more traditional technique utilizing a bone transducer operated at a supraliminal level.

Lastly, a “meta-earplug” push-to-fit foam earplug, denoted as “Meta-EP,” is featured in this investigation. This earplug was developed by our research team to mitigate the occlusion effect [8]. It relies on critically coupled Helmholtz resonators organized in parallel. As detailed in [8], three variants of the Meta-EP are examined: (1) all resonators active, (2) no resonators active, and (3) only one resonator active. The primary objectives of introducing this occlusion device are twofold: firstly, to validate that the proposed ATF effectively captures the earplug’s impact even with shallow or moderately deep insertions. This is particularly pertinent for occlusion devices where the acoustic impedance of their medial surface (i.e., the surface facing the tympanic membrane) has been optimized for OE mitigation. Secondly, to ascertain if the outcomes from [8] are replicated despite modifications to the boundary conditions applied to the truncated ear (i.e., from a bonded top bony part in [8] to a free condition of the same surface in this work).

All earplugs were pre-compressed to facilitate insertion into the artificial earcanal, except for the home-made silicone one and the Multi-flange polymer earplug. To achieve this, a hand-actuated crimper from Blockwise [30] was employed. This device provides a level of control over pre-compression, thereby minimizing the variability in insertion that manual compression of an earplug could introduce [31]. Lastly, a thin layer of Vaseline was applied to the earplugs before insertion, with the exception of the earplugs belonging to the “roll-down foam” family.

In the case of the validation phase using the silicone earplug, four repetitions are taken for each test by removing and repositioning the artificial ear prototype and earplug in order to account for the variability associated with mounting conditions (e.g., positioning of the prototype and fitting of the earplug). For all tests conducted on commercial earplugs, a minimum of three measurements are taken, each with a new earplug. In the case of home-made earplugs, typically only one earplug is

Table 1
Reference names of the earplugs considered in this study.

Earplug family	Custom-molded	Roll-down-foam		Multi-flange elastomeric polymer	Push-to-fit foam			
Picture								
Earplug model manufacturer’s name	Home-made	3 M™ E-A-R™ Classic regular	Honeywell Howard Leight Max regular	3 M™ E-A-R™ UltraFit™	Home-made earpiece with a Comply eartip	3 M™ E-A-R™ Push-Ins	Honeywell TrustFit® Pod	Home-made
Label used in this study	Silicone	Cylindrical foam	Bell-shaped foam	Multi-flange polymer	Push-to-fit foam pod 1	Push-to-fit foam pod 2	Push-to-fit foam pod 3	Meta-EP
Insertion depth	Shallow (6 mm)	Shallow (5 mm), medium (10 mm), deep (15 mm)	Medium (10 mm), deep (15 mm)	Medium (12 mm)	Medium (11 mm)	Medium (10 mm)	Medium (10 mm), deep (15 mm)	Medium (11 mm)

available and is removed from the ear between each measurement.

4. Virtual tester

The proposed virtual tester is built upon the ATF and features a FE model of its vibroacoustic behavior. This section outlines the associated geometry, material properties, loading and boundary conditions, meshing, solving, and the vibroacoustic indicators of interest. These indicators are also measured using the ATF and utilized for the validation phase of the virtual tester.

4.1. Geometry

The FE modeling is carried out based on the geometry of the truncated ear already described in Section 2. This geometry is the one sent to the ear prototype manufacturer. It has a parallelepipedic shape whose dimensions are 28.4 mm (width), 38.4 mm (height) and 37 mm (length), respectively (see Fig. 1(a)). The earcanal cavity is a simple cylindrical tube with a constant cross-section diameter of 6.6 mm and a length of 30 mm. The cartilage is a ring-shaped domain around the earcanal cavity and encased in the soft tissues. Its length is 11 mm along the earcanal cavity, and its thickness is 3.1 mm. The distance between the cartilage and earcanal cavity is about 1.9 mm. The earcanal cavity walls are made of soft tissues. The thickness of the soft tissue layer surrounding the posterior “bony” part of the earcanal cavity is 1 mm. The probe-tube at the eardrum position is not modeled, and the earcanal terminates with a bony surface at the position of the tympanic membrane. The top accelerometer is also omitted from the model due to its negligible mass compared to that of the artificial ear.

The earplug studied in the validation phase of the numerical model is a custom-molded silicone earplug of a cylindrical shape (see section 3.3). Its total length is 14 mm, and its diameter is chosen to be equal to the earcanal diameter for the design geometry (see yellow domain in Fig. 4). This type of earplug is adopted since it has been used in the authors’ previous numerical work, and has provided a satisfactory simulation result of sound attenuation compared with experimental data [32]. The length of the inserted part of the earplug is about 6 mm, which corresponds to a shallow insertion. This insertion depth can offer a more pronounced OE compared with a medium or deep insertion (e.g., [12,18]). The deformation of the soft tissue that may be induced by the insertion of the earplug is not accounted for. The inserted part of the earplug is considered to perfectly fit the original shape of the earcanal (see also yellow domain in Fig. 4). Additionally, the excitation plate is considered in the FE model, which is in direct contact with the soft tissues (see Fig. 4). Its diameter and thickness are 140 mm and 6.4 mm, respectively. The use of a plate allows to control the noise produced by the excitation system and replicate it within the virtual tester. Indeed, the open ear configuration is the trickiest one since by definition it impacts significantly the OE (i.e., the OE decreases with the increase of the sound pressure level in the open ear) and it can be altered experimentally by noise sources which are difficult to take into account in the model (i.e., the shaker, the ventilation system, external noises passing

through the walls of the audiometric booth). The other parts of the test bench are not included for simplicity.

4.2. Material properties

In the FE model, the earcanal cavity and external air domains are assumed to be perfect compressible gas domains characterized by their density ($\rho_0 = 1.2 \text{ kg/m}^3$) and speed of sound in air ($c_0 = 343.4 \text{ m/s}$) under standard conditions for temperature and atmospheric pressure. Indeed, preliminary numerical tests have shown that thermal and viscous dissipations do not make any difference to the simulation results and energy losses are thus neglected in these domains. The other components are all modeled as linear isotropic elastic solids, whose mechanical properties, i.e., density (ρ_s), Young’s modulus (E_s), Poisson’s ratio (ν_s), structural loss factor (η_s), are either taken from the literature (see Table 2) or characterized in the laboratory (see section 3.2).

The excitation plate is made of normal structural aluminum, and the built-in material properties in COMSOL Multiphysics (v.6.1 COMSOL®, Sweden) are used. The bony part is made of epoxy-based composite material as mentioned in Section 2. Its mechanical properties are adopted from the work of Benacchio et al. [33]. The properties of the silicone earplug have already been characterized in an authors’ previous work [32], and are provided in Table 2 as well. The cartilage and soft tissues are both made of urethane-based soft resins. The mechanical properties of the cartilage is adopted from the work of Benacchio et al. [33]. The ones of the soft tissue material are characterized with the experimental setups presented in section 3.2 and values provided in section 6.1.

4.3. Loading and boundary conditions

The artificial ear and vibrating rigid plate geometries are imported in the FE software and surrounded by an air-filled convex domain and a perfectly matched layer (PML), which simulates the Sommerfeld condition (see Fig. 4 (a)). The loading and boundary conditions in the FE model are chosen to best correspond to the test bench used for experimental measurements (see Section 3). First, a dynamic displacement with an amplitude of 1 mm is imposed on a circular area with a diameter of 19 mm in the center of the bottom surface of the excitation plate (x direction); the displacements along y and z directions are blocked (see Fig. 4(b)). Second, the symmetry of the problem (i.e., geometry, loading and boundary conditions) with respect to the (x,y) plane allows for modeling only half of the system, and thus reducing the computational

Table 2
Solid material properties used in the FE model.

	Excitation plate	Bone	Cartilage	Earplug Silicone
ρ_s [kg/m ³]	2700	2267	1075	1500
E_s [kPa]	7×10^7	1.36×10^7	1.647×10^3	2.9×10^3
ν_s [1]	0.33	0.31	0.478	0.49
η_s [1]	0.005	0.01	0.05	0.1

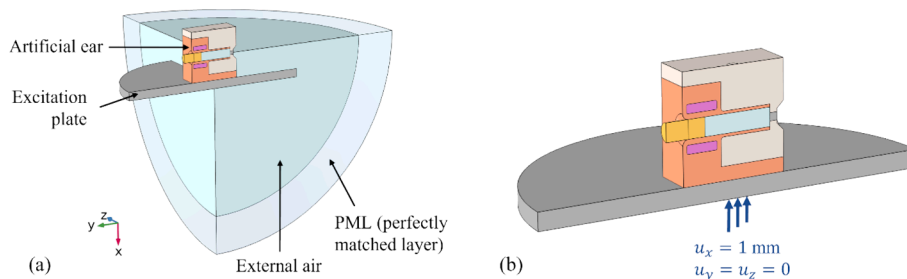


Fig. 4. FE model of the system: (a) global view, half artificial ear placed in an external air domain surrounded by a PML; (b) zoomed-in view, half artificial ear on an excitation plate subjected to prescribed displacement conditions.

cost. The symmetry condition is achieved by (i) blocking the displacement along the z -direction on the solid boundaries and (ii) imposing rigid boundary conditions on the fluid boundaries. Third, the fluid–structure coupling condition applies at the other interfaces between solid and fluid domains (i.e., continuity of tractions and normal displacements), such as the exterior boundaries of the artificial ear in contact with the external air domain. Continuity of stresses and displacements is assumed at solid–solid interfaces, such as the interface between the bony part and soft tissues.

4.4. Meshing and solving

All the domains in the FE model except for the PML are meshed using 10-noded tetrahedral elements, whereas the PML is meshed with 15-noded quadratic triangular prisms. A convergence criterion of at least 4 elements per wavelength is chosen in order for the mesh to capture the system response with a desired accuracy. The FE problem is solved using commercial software COMSOL Multiphysics (v.6.1 COMSOL®, Sweden). The calculations are performed in narrow frequency bands from 100 Hz to 1250 Hz with a 10 Hz step. Third-octave band responses are then obtained from narrow band results using a MATLAB routine (MATLAB 2023a, MathWorks, Inc., USA) based on ANSI S1.11 standard [34].

5. Vibroacoustic indicators

The OE is determined from the transfer functions between the average sound pressure p assessed over the probe-tube outer surface and the acceleration at the center of the excitation plate acc_{plate} such as:

$$OE = 20 \log_{10} \left(\frac{H_{p,acc_{plate}}^{occ}}{H_{p,acc_{plate}}^{open}} \right) \quad (1)$$

$H_{p,acc_{plate}}^{open}$ and $H_{p,acc_{plate}}^{occ}$ denote the transfer functions in the open and occluded configurations, respectively. In the case of the FE model, the simulated acceleration is simply obtained by multiplying d the displacement excitation imposed on the excitation plate by $-\omega^2$. The transmissibility is determined from the transfer function between the acceleration at the center of the top “bony” surface of the ATF acc_{top} and the acceleration at the center of the excitation plate acc_{plate} :

$$T = 20 \log_{10} \left(\left| H_{acc_{top},acc_{plate}}^i \right| \right) \quad (2)$$

where $i \in \{\text{open, occ.}\}$ since the transfer function can be measured in both open and occluded conditions of the ATF.

6. Results and discussion

6.1. Mechanical properties of the soft tissue material

The density of the soft tissue material is $\rho_s = 1007 \text{ kg/m}^3$. Its mechanical properties (E_s , ν_s , η_s) determined from the three different techniques are shown in Table 3. The mechanical properties are categorized into three sets: set#1 for compression, set#2 for tensile, and set#3 for transmissibility methods. Remarkably, both compression and tensile methods yield comparable values for Young’s modulus and Poisson’s ratio, instilling confidence in the accuracy of the provided data

Table 3
Mechanical properties of the soft tissue material.

	Set#1	Set#2	Set#3
Characterization method	Compression (QMA)	Tensile	Transmissibility
E_s [kPa]	1.312×10^2	1.5×10^2	1.5×10^2
ν_s [1]	0.478	0.46	0.493
η_s [1]	0.072	–	0.15

and the robustness of the characterization procedures.

Fig. 5 illustrates both the measurements and simulations of acceleration transmissibility within specific frequency bands ranging from 100 Hz to 1000 Hz, with a frequency increment of 10 Hz in the case of the simulations. This figure reveals that the simulations of acceleration transmissibility, generated by the virtual tester utilizing the set#1 and set#2 of soft tissue mechanical properties (depicted by the solid blue and green curves), fail to accurately replicate the vibratory behavior observed on the ATF (illustrated by the solid black curve). The transmissibility maxima at low frequencies exhibit discrepancies—falling below the desired frequency range and surpassing the expected amplitude levels when compared to the measurements. Note that since the tensile method does not provide the loss factor, the latter for set #2 is assumed equal to that of set #1.

Within the “transmissibility” characterization technique, calibration of the mechanical properties for the soft tissue material of the virtual tester involves manual adjustments to align the transmissibility simulation with the actual measured data. The simulation corresponding to set#3 is depicted by the solid red curve in Fig. 5. The amplitude of the primary peak at 200 Hz serves as a basis for determining the structural loss factor (η_s) of the soft tissue material. Additionally, the frequencies of the two transmissibility peaks, observed at 120 Hz and 200 Hz, contribute to establishing both the Young’s modulus (E_s) and Poisson’s ratio (ν_s). Upon scrutinizing the simulations depicting the magnitude of artificial ear displacement in Fig. 5 (c), it is apparent that the initial peak transmissibility at 120 Hz is primarily associated with rotational displacement around the z -axis, while the subsequent peak at 200 Hz corresponds to the classical “pumping motion,” predominantly involving displacement along the x -axis, aligned with the motion of the excitation plate. Utilizing the transmissibility technique, the Poisson’s ratio is increased to 0.493, demonstrating its significant influence on the vibratory behavior of the ear in this frequency range. This adjustment is crucial for accurately predicting the two transmissibility peaks. Additional simulations (not presented here for brevity) indicate that, if the Poisson’s ratio is held constant at 0.478, the Young’s modulus must be increased to 1.9e2 kPa to properly fit the second transmissibility peak. However, in this case, the first peak is overestimated both in frequency and amplitude. Moreover, the Young’s modulus derived from the transmissibility technique (set#3, with $\nu_s = 0.493$) aligns with the value obtained from the tensile technique (set#2), reinforcing confidence in the accuracy of the data obtained. As expected, the simulation generated by the virtual tester using set#3 for the soft tissue material’s mechanical properties offers a good estimation of the transmissibility observed on the ATF up to 500 Hz. Discrepancies between the model and measurements at higher frequencies can be attributed to the oversight that the mechanical properties of the material increase with frequency—an aspect not currently considered in the model.

6.2. Numerical evaluation of the ATF

This section is mainly dedicated to validating the virtual tester through a comparative analysis of its vibro-acoustic outputs with measurements conducted on the ATF, specifically accounting for the shallow insertion of the silicone earplug. Complementary numerical analyses are proposed to enhance understanding of the physical phenomena underlying the observed vibroacoustic behavior of the proposed ATF and which explain the evaluated OE.

6.2.1. Open ear

Fig. 6(a) presents the vibroacoustic transfer function of the open ear $H_{p,acc_{plate}}^{open}$: simulation result based on the soft tissues set#3 (solid red curve) alongside experimental data obtained on the ATF (solid black curve). Results are displayed in narrow frequency bands from 100 Hz to 1000 Hz (with a frequency step of 10 Hz for the simulations). The transfer function exhibits an ascending frequency response with a

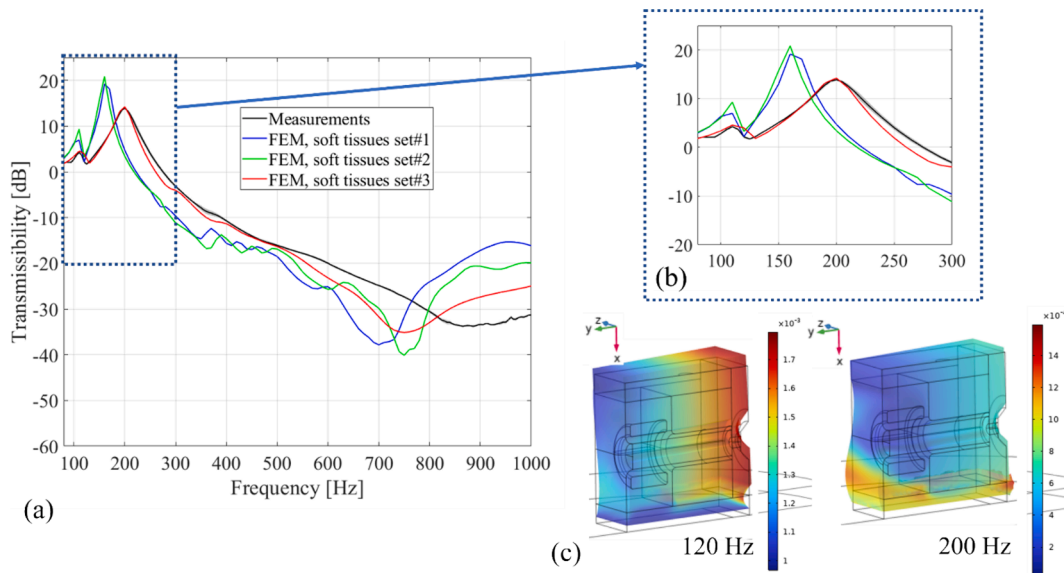


Fig. 5. (a) Measurement and simulations of the acceleration transmissibility (Eq. (2)); (b) zoom between 80 Hz and 300 Hz and (c) simulations of the magnitude displacement of the artificial ear at 120 Hz and 200 Hz (only one half of the ear is displayed, a result of the symmetry plane employed in the model).

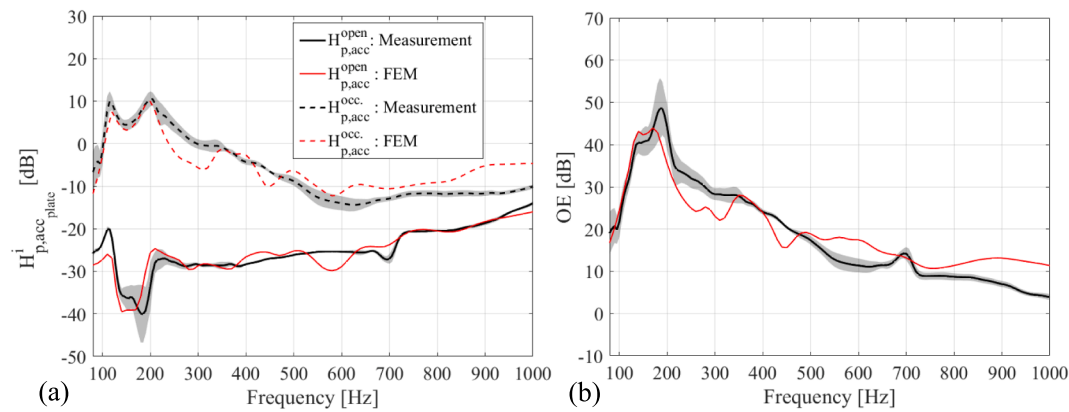


Fig. 6. Comparison between the simulation and measurement results: (a) transfer functions for open and occluded ears, and (b) OE. Simulation results based on the soft tissues set properties #3 are presented using the red lines; measurement results are presented using the black lines (mean \pm standard deviation in grey).

pronounced drop between 120 Hz and 200 Hz (associated to the artificial ear resonances presented in Fig. 5(b)). The shaded region in gray denotes the measurement variability, particularly notable within this frequency range. It is noteworthy that the adhesive fixation quality, realized through double-sided tape, significantly impacts $H^i_{p,acc}$ within this specific frequency band ($f < 200$ Hz), necessitating periodic replacement. The virtual tester, utilizing set#3 for the mechanical properties of the soft tissue material, accurately predicts $H^i_{p,acc}$ across the entire frequency range of interest (see red curve). The virtual tester is subsequently employed to gain a deeper understanding of the trends observed in Fig. 6(a). The objective is to determine if the bone-conduction pathway involving the radiation of the ear canal walls dominates the sound pressure at the eardrum, as would be expected for an outer ear excited by bone conduction.

To determine which pathway, air-conduction or bone-conduction, dominates the sound pressure level generated in the open ear, four supplementary configurations are computed using the virtual tester. These four configurations are based on coupling only specific surfaces of the ATF with the surrounding air to isolate their contribution: the bone-conduction pathway BC#1 involves the contribution of the ear canal wall surface only; the bone-conduction pathway BC#2 involves the surrounding soft tissue surface only; the bone-conduction pathway

BC#3 involves the bony surface at the eardrum position only; and finally, the air-conduction pathway AC involves the excitation plate surface only. Note that the sum of all contributions, both in amplitude and phase, equals the baseline configuration where the system is fully coupled (i.e., all ATF surfaces are coupled to the surrounding air) by means of the superposition principle. Fig. 7 displays the sound pressure level induced by these 4 contributions (AC, BC#1-BC#3) together with the one induced by the base configuration (solid black curve). It is shown that the AC pathway dominates the BC pathways in the whole frequency range of interest, with only two exceptions at 120 Hz and 200 Hz, corresponding to the structural modes of the system. Below 200 Hz, BC#3 (involving the surface at the eardrum position) significantly contributes to the open ear sound pressure level. However, it does so in phase opposition to the excitation plate (not shown here for conciseness), which explains the observed sound pressure drop at low frequencies (i.e., between 100 Hz and 200 Hz). Interestingly, BC#2 is the main BC contributor at the pumping motion resonance (around 200 Hz) whereas above 600 Hz, it is BC#1 (even if AC dominates). The fact that the AC pathway dominates the sound pressure level of the open ATF may lead to an underestimation of the OE compared to measurements on participants generated by an *a priori* less noisy bone transducer (see section 6.3.1). On the other hand, as mentioned previously, having an

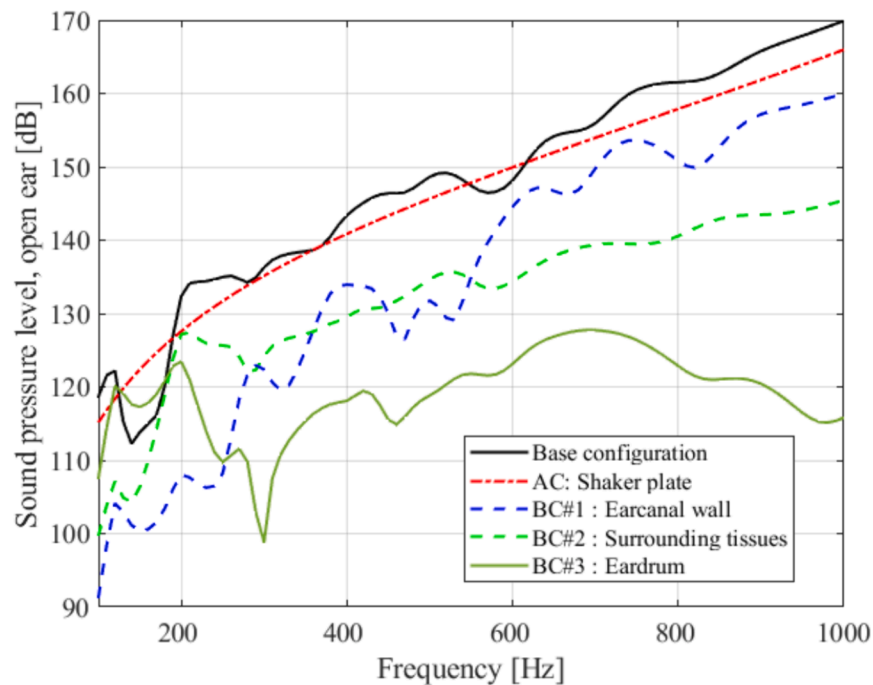


Fig. 7. Sound pressure level in the open ear when the system is fully coupled (base configuration) and when specific surfaces of the ATF are coupled to the surrounding air (leading to the AC and BC#1-BC#3 contributions).

excitation plate allows to control the main noise source in the open ear (other uncontrolled sources, such as the shaker, are masked during the experiments) and simulate it.

6.2.2. Occluded ear

Fig. 6(a) and (b) respectively present the transfer function in the occluded ear $H_{p,acc_{plate}}^{occ}$ (see dashed black and red curves) and the OE (see Eq. (1)). As expected, the sound pressure level in the occluded ear is highly increased compared to the open case, illustrated by the amplitude of $H_{p,acc_{plate}}^{occ}$ which highly and consistently surpasses that of $H_{p,acc_{plate}}^{open}$ (see Fig. 6(a)). This results in a computed OE exceeding 0 dB across the entire frequency range of interest (see Fig. 6(b)), with a maximum around 50 dB close to 200 Hz and a decrease of approximately 40 dB/decade. Once again, the virtual tester associated with the soft tissues set#3 satisfactorily predicts the $H_{p,acc_{plate}}^{occ}$ and the OE, thereby confirming its validation.

The behavior of the OE obtained with the proposed ATF occluded by a shallowly inserted earplug is as expected for this type of occlusion device [7,18]: i.e., significant amplitude in low frequencies and a decrease of 40 dB/decade. The decrease of the OE in frequency by 40 dB/decade, is caused by the change in impedance seen by the cavities' vibrating walls, which is dominated by inertial effects in an open ear (the impedance increases with a slope of +20 dB/decade) and by compressibility effects in an occluded ear (the impedance decreases with a slope of -20 dB/decade). Fig. 11 of Appendix A shows, via the virtual tester, that the proposed ATF indeed replicates these two behaviors. The amplitude of the OE in low frequencies (taken at the peak of the OE frequency curve) is known to depend greatly on boundary conditions and the loading case applied to the truncated ear (see Figs. 10 and 12 of reference [7]) and very likely on the geometry of the outer ear (e.g., shape of the earcanal, thickness of tissues, and position of the cartilage). Indeed, these parameters affect the vibratory behavior of the earcanal walls and of the earplug, which are the source of the OE. Therefore, the ability of this ATF to realistically reproduce the vibrational field of the earcanal walls, particularly at the low-frequency resonances of the ear

($f < 200$ Hz), is questionable. At the resonance frequencies of the ATF, the pressure in the occluded canal is significant (see the two maxima of $H_{p,acc_{plate}}^{occ}$ below 200 Hz in Fig. 6(a)) due to the important vibration amplitude of the earcanal walls; and which can be overestimated compared to a real human ear under bone-conducted stimulation. This can lead to an overestimation of the OE, especially since the open ear transfer function shows a drop below 200 Hz for the reasons explained earlier in section 6.2.1. One approach to eliminate these resonances that generate significant ear vibration is to bond the top "bony" part of the truncated ear. Appendix B presents measurements and numerical simulations that have been performed to explore the influence of the boundary condition applied to this top bony side. In the current version of the ATF, it is shown that leaving the ear free on the top reduces the modal behavior of the test bench and measurement variability, and thus improve OE assessment and ease the validation of the virtual tester.

6.3. Experimental evaluation of the ATF

This section further evaluates the proposed ATF. Supplementary measurements are undertaken to assess the ATF's ability to reproduce the OE measured on real human ears, as well as to determine if it can distinguish the influence of different earplugs and their insertion depth on the OE.

6.3.1. Comparison with human participant

Fig. 8 presents the OE of the Push-to-fit foam pod 1, a home-made earpiece previously investigated in [29], where OE measurements were collected from a group of participants. It is shown that ATF measurements mostly fall within the inter-individual variability observed in the group of participants and which is likely attributable to inherent variations in earcanal morphology. This suggests that the proposed truncated ear can be deemed representative, even if it does not provide the average OE obtained from all participants (depicted by the solid black curve).

The discrepancies at low frequencies ($f < 200$ Hz) may originate

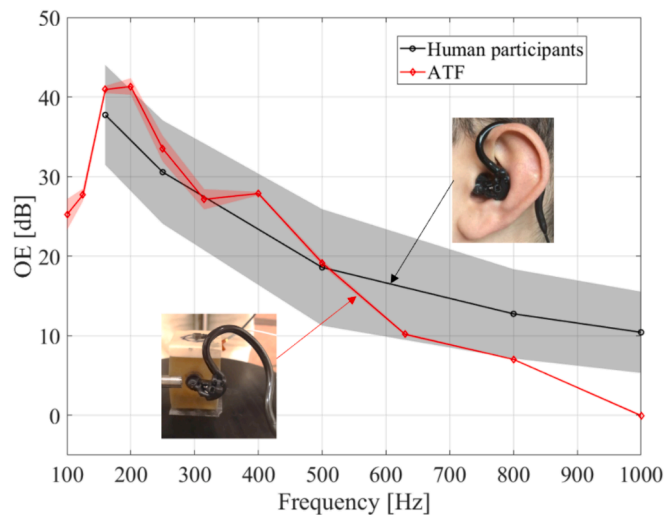


Fig. 8. Occlusion effect (mean \pm standard deviation) induced by the Push-to-fit foam pod 1 measured on human participants and with the proposed ATF.

from the artificial ear resonances which are not representative of the head dynamics at low frequency. Bonding the top bony surface of the ear indeed could reduce the OE at low frequencies as shown in Appendix B. Furthermore, the underestimation of the OE above 800 Hz may be attributed to the substantial airborne contribution observed in the open ear canal configuration of the ATF, as discussed in section 6.2.1. Indeed, the noise level in the open ATF is dominated here by the excitation plate's radiation and thus does not correspond to a case of pure bone conduction that mainly occurs for a bone transducer excitation. The latter effect can be more detrimental for frequencies above 800 Hz, where the amplitude of the open ear transfer function is of the same order of magnitude as the one of the occluded ear canal (see Fig. 6(a)). Nevertheless, this significant contribution of the open ear to the OE raises questions about the possibility of comparing literature data obtained from participants with each other, as well as with simulation results. Indeed, it is highly likely that the background noise, which primarily contributes to the sound pressure level in the open ear canal (considering that the noise level radiated by the bone transducer is low), is not the same from one measurement environment to another, and that its effect is hidden in the OE curve. This measurement of the open ear thus fully contributes to the variability of OE measurements in the literature. Therefore, another method for assessing the OE should be preferred, such as the 'NR-based method' investigated in [29] which only uses the occluded ear configuration. However, this is beyond the scope of this paper.

One might also question the need for the cartilage component in the ear to enhance its realism. To provide some answers, Appendix C proposes a numerical study based on the use of a virtual tester to evaluate the sensitivity of the OE to the presence and position of the cartilaginous component. This study is conducted for the two boundary conditions on the top bony surface of the ear (i.e., free and bonded). The numerical study reveals that the absence of cartilage significantly increases the OE at low frequencies (mainly due to an increased volume velocity of the ear canal walls in the occluded ear configuration), irrespective of the boundary condition applied to the top bony side of the ear. The presence of cartilage thus appears to be relevant for this ear, as otherwise, the OE would have been significantly higher than the average of the participants at low frequencies based on the results of Fig. 8. Furthermore, the numerical study of Appendix C shows that the cartilage's position within the soft tissue demonstrates an influence only when the artificial ear's top bony side is bonded and at low frequencies ($f < 500$ Hz). Should future measurements on human participants confirm that the cartilage's outer ear anatomy is a key factor in inter-individual variability in both

objective OE and experienced OE, the boundary conditions of the next generation ATF will need adjustment to accurately capture this effect.

6.3.2. Effect of the earplug at a medium insertion depth

Fig. 9 presents the OE measured on a diverse range of earplugs, encompassing both commercial and home-made variants as detailed in Table 1. The measurements were conducted with a medium insertion depth, specifically around 10 mm, with variations depending on the tested earplug (ranging from 10 mm to 12 mm, as indicated in Table 1). In Fig. 9(a), the OEs of different commercial earplugs are depicted. Remarkably, the OEs of the tested commercial earplugs are tightly grouped, all falling within the observed inter-individual variability of the participant group using the Push-to-fit foam pod 1. Given the distinct geometries and materials of these earplugs, one might have anticipated more pronounced differences in their OEs. Indeed, previous research [18] indicated that the influence of the earplug on the OE increases with insertion depth (explained by the augmentation of the relative contribution of the medial earplug surface in terms of volume velocity compared to that of the free ear canal wall coupled to the occluded ear canal cavity), suggesting that differences in OE among earplugs could manifest even at a medium insertion depth. On the other hand, this result may not be surprising, as "disposable and reusable" commercial earplugs are primarily designed to provide effective noise protection for a broad population, rather than specifically addressing the occlusion effect. Nevertheless, Fig. 9(a) shows that the two roll-down foam earplugs (represented by the blue and pink curves) exhibit a lower OE within the frequency range of 200 Hz to 600 Hz. This observation aligns with the findings of a previous study [18], which concluded that earplugs featuring a low Poisson's ratio, such as roll-down foam, result in decreased volume velocity at the medial earplug surface, consequently reducing the OE.

To ascertain the capability of the proposed ATF in capturing the impact of an earplug on the OE at a medium insertion depth, the Meta-Earplug (Meta-EP) introduced in [8] was assessed. Following the methodology outlined in [8], three variants of the Meta-EP were investigated, and the OE results are presented in Fig. 9(b), corresponding to the conditions where (1) all resonators are active (black curve), (2) no resonators are active (red curve), and (3) only one resonator is active (blue curve). Noteworthy distinctions emerge among the three Meta-EPs, as well as between these earplugs and the commercial ones showcased in Fig. 9(a). Specifically, the Meta-EP with all resonators active exhibits an OE below 5 dB beyond 400 Hz, a level not attained by any of the commercial earplugs at such frequencies. Finally, the OE of these 3 Meta-EPs measured on the proposed ATF (Fig. 9(b)) are consistent with those obtained on a previous version of the ATF where the top of the ear was bonded (see Fig. 4(b) of [8]). The main differences are concentrated in the low-frequency ($f < 180$ Hz) and high-frequency ($f > 800$ Hz) ranges, as discussed in greater detail in Appendix B.

6.3.3. Effect of the insertion depth

The effect of the insertion depth on the OE measured by the ATF is investigated for three commercial earplugs (see Fig. 10): (a) the cylindrical roll-down foam earplug, (b) the bell-shaped roll-down foam earplug and (c) the push-to-fit foam pod 3 earplug. A decrease of the OE with the insertion depth is observed for the cylindrical foam and the Push-to-fit foam pod 3 earplugs (see Fig. 10(a) and 10(c)). As mentioned in [18], this effect is due to the decrease in the free ear canal wall normal velocity with insertion depth. The bell-shaped design of the orange roll-down foam earplug may account for the absence of an observed insertion depth effect for this earplug. Indeed, the conical/rounded-shaped tip for the medial portion of the earplug reduces the area of the earplug in contact with the soft tissue for a given insertion depth (measured from the most medial part of the earplug). Finally, it is found that the contrast in OE between the earplug types is more prominent with a 15 mm insertion depth (see Fig. 10(d)) than with a 10 mm insertion depth (see Fig. 9(a)). This outcome is anticipated and is likely

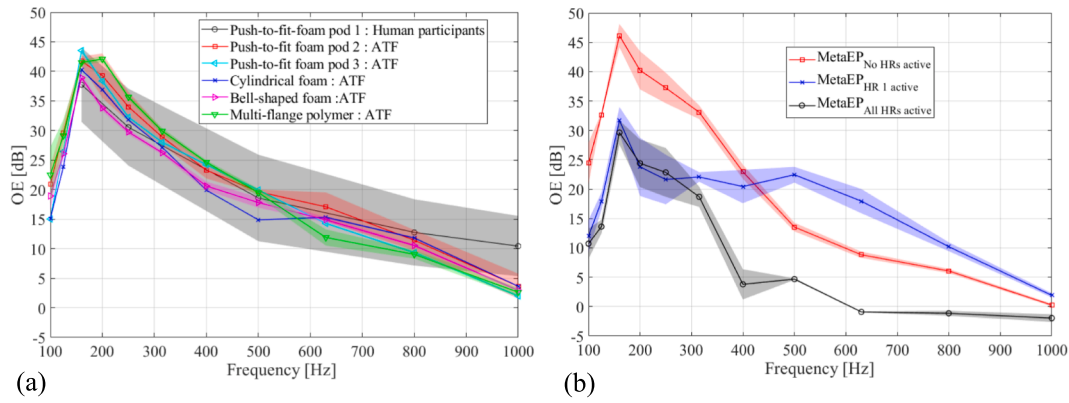


Fig. 9. Occlusion effect (mean \pm standard deviation) induced by various types of earplugs at medium insertion depth (around 10 mm) and measured with the proposed ATF; (a) commercial earplugs; (b) Meta-EP with all HRs active, no HRs active and only HR#1 active. Results are presented in 3rd octave bands.

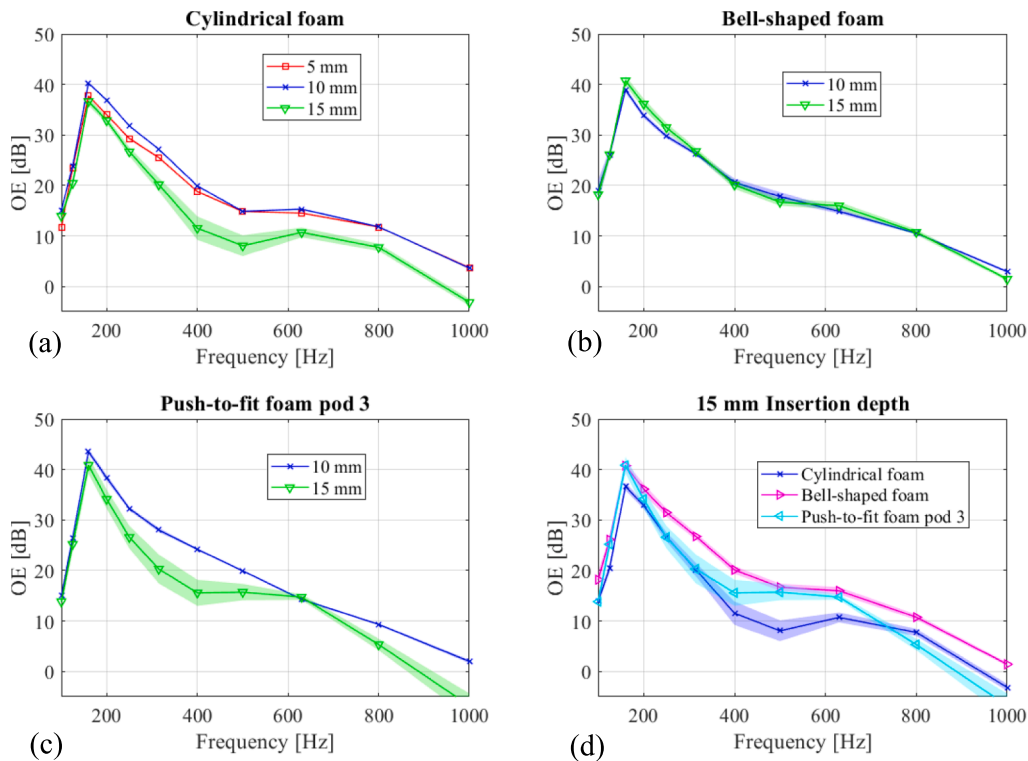


Fig. 10. Occlusion effect (mean \pm standard deviation) induced by 3 different commercial earplugs and for different insertion depths (5 mm, 10 mm or 15 mm): (a) the cylindrical roll-down foam earplug, (b) the bell-shaped roll-down foam earplug and (c) the push-to-fit foam pod 3 earplug; (d) this three commercial earplugs at the same 15 mm insertion depth.

associated with the volume velocity of the medial earplug surface, which is expected to differ due to the distinct geometry and material of these two earplugs [18].

7. Conclusion

This paper introduces an acoustical test fixture (ATF) centered on an artificial truncated ear for the quantification of the objective occlusion effect (OE) induced by earplugs. In contrast to standardized ATFs designed for sound attenuation measurements in hearing protection devices, the proposed ATF employs a more anatomically realistic truncated ear, incorporating soft tissues, cartilage, and bone components to replicate the outer ear bone conduction path crucial for OE assessments. Various ATF components, including outer ear geometry, acoustical and mechanical boundary conditions, and loading, are meticulously chosen

to facilitate the development and validation of a computationally efficient Finite Element (FE) method-based virtual tester. It is shown that the proposed ATF can reproduce key effects observed in objective OE measurements on human participants: (i) significant OE at low frequencies, diminishing with increasing frequency, (ii) reduction of OE with greater insertion depth, and (iii) distinctions among various earplug types, particularly noticeable at deeper insertions compared to shallow ones. This ATF can therefore be used to design in-ear devices with a reduced occlusion effect, leading to an improved experience for many users of hearing protectors, hearing aids, and earbuds.

A significant achievement of this study is the validation of the virtual tester, specifically under conditions of occlusion caused by a custom-made silicone earplug with shallow insertion. The validation process involved a comprehensive characterization phase of the synthetic materials used to replicate soft tissues. This validated virtual tester was

used to further investigate the vibroacoustic behavior of the ATF and to understand the main physical phenomena leading to the OE. It can also be used in future research to re-evaluate ATF design parameters and improve OE assessment.

Note

All the authors certify that all of them have seen and approved the final version of the manuscript being submitted. They warrant that the article is the authors' original work, hasn't received prior publication and isn't under consideration for publication elsewhere.

Declaration of Generative AI and AI-assisted technologies in the writing process

During the preparation of this work the authors used GPT-3.5 (OpenAI, 2021), retrieved from <https://openai.com>, in order to enhance the text's coherence, grammar, and syntax. After using this tool/service, the authors reviewed and edited the content as needed and take(s) full responsibility for the content of the publication.

CRediT authorship contribution statement

Olivier Doutres: Writing – review & editing, Writing – original draft, Validation, Supervision, Software, Project administration, Methodology, Investigation, Funding acquisition, Formal analysis, Conceptualization. **Yu Luan:** Writing – review & editing, Writing – original draft, Validation, Methodology, Investigation, Formal analysis, Conceptualization. **Marc-Olivier Cyr-Desroches:** Writing – review &

editing, Validation, Methodology, Investigation, Formal analysis. **Kévin Carillo:** Writing – review & editing, Validation, Software, Methodology, Investigation, Formal analysis, Conceptualization. **Robin Richert:** Writing – review & editing, Validation, Investigation, Formal analysis. **Franck Sgard:** Writing – review & editing, Supervision, Software, Methodology, Funding acquisition, Conceptualization.

Declaration of competing interest

The authors declare that they have no known competing financial interests or personal relationships that could have appeared to influence the work reported in this paper.

Data availability

Data will be made available on request.

Acknowledgements

The authors wish to dedicate this work to the memory of their colleague and friend Simon Benacchio, who passed away far too soon in 2023. It was a true pleasure collaborating with him on this subject since 2015. The authors acknowledge the support of the Institut de Recherche Robert-Sauvé en Santé et en Sécurité du Travail (IRSST) (Funding Reference No. 2015-0014) and the MITACS Accelerate program (Funding Reference No. IT10643). Authors would like to thank Elisabeth Laroche (LIO-HSCM, ÉTS) and Éric Wagnac (LIO-HSCM, ÉTS) for the tensile test measurements.

Appendix A. . Acoustic impedance seen by the earcanal walls

The acoustic impedance seen by the vibrating earcanal wall in both open and occluded cases is computed numerically using the virtual tester and the following expression:

$$Z_{EC}^i = \frac{p_{EC,wall}^i}{q_{EC,wall}^i} \quad (3)$$

where $i \in \{\text{open}, \text{occ.}\}$, $p_{EC,wall}^i$ is the surface averaged acoustic pressure while $q_{EC,wall}^i$ is the total volume velocity flowing through the earcanal wall. In the two configurations used to compute this indicator (i.e., open and occluded), only the earcanal walls were coupled to the fluid in the earcanal cavity (note that in the case of the open ear, the configuration is the same as the one used to compute BC#3 in section 6.2.1). Fig. 11 displays the acoustic impedance seen by the earcanal walls in both open and occluded cases. The level of the earcanal cavity acoustic impedance increases with frequency by approximately +20 dB/decade in the open case, while it decreases with frequency by approximately -20 dB/decade in the occluded case. These curves are typical of the inertia effect in the open case and the compressibility effect in the occluded case [7].

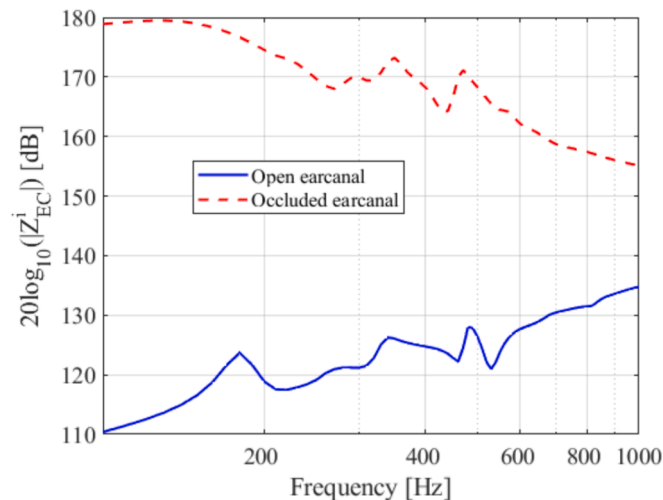


Fig. 11. Acoustic impedance level in dB (ref. 1 N.s.m⁻⁵) seen by the earcanal wall in both open and occluded cases.

Appendix B. . Effect of the boundary conditions

The influence of the boundary condition applied to the top bony side of the truncated ear is investigated. The examination of the boundary condition's influence is important since (i) it is complex to select an appropriate mechanical boundary condition for a truncated ear and (ii) it can have a significant impact on relevant vibroacoustic indicators, as emphasized in previous research [7]. As for the virtual tester (see Fig. 12(a)), the sole modification from the original model (presented in section 4) lies in the boundary condition applied to the top side of the ear. In this instance, displacements along the x , y and z directions are constrained at the ear's top surface. The static compression experienced by the artificial ear is indirectly considered through the mechanical properties of the soft tissues, assumed to be 0,8 % in this case (see Table 3).

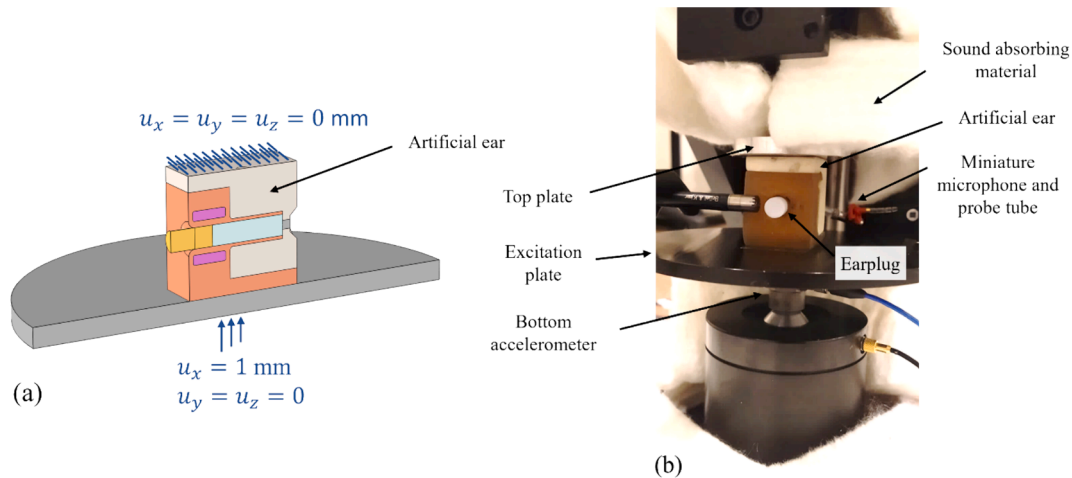


Fig. 12. Bonded boundary condition at the top bony side of the ear: (a) virtual tester (b) ATF with a compressed ear between two plates.

In the case of the ATF (see Fig. 12(b)), the artificial ear undergoes compression between the excitation plate and a rigid top plate affixed to the structure of the QMA. The top bony side of the ear is secured to this plate using double-sided tape. A worm screw facilitates the control of the rigid plate's static position, thereby regulating the compression of the artificial ear. However, the ATF lacks a system to precisely determine the plate's position, making it challenging to ascertain the exact static compression applied to the ear. Due to the non-parallel alignment of the bottom and top sides of the parallelepipedic ear, the nominal position of the top plate is established when full contact is achieved between the top side of the ear and the plate (determined by visual inspection), covering the entire surface of the ear's top side. To accommodate the lack of precise control over ear compression, multiple measurements were conducted by slightly adjusting the top plate around its nominal position (static compression of $\pm 0,8\%$ around the nominal thickness of the ear). The influence of this variation will be evident in the results, as illustrated by the standard deviation plotted around the mean value.

As in section 6.2, the three indicators of interest are: the vibroacoustic transfer functions of the open ear ($H_{p,acc_{plate}}^{open}$) and occluded ear ($H_{p,acc_{plate}}^{occ}$), as well as the OE (see Eq. (1)). Fig. 13 presents experimental data obtained on the modified ATF (solid black curves), alongside simulation results based on the set#3 (solid red curves). For comparison, the experimental data from the original ATF (i.e., with the top of the ear left free) and simulations using with the corresponding original virtual tester are presented (depicted by dashed black and red curves, respectively). The experimental findings reveal a significant influence of the boundary condition on the vibroacoustic behavior of the occluded ATF, evident in both low-frequency ($f < 400$ Hz) and high-frequency ($f > 650$ Hz) ranges. When the top side of the ear is bonded, the transfer function of the occluded ear ($H_{p,acc_{plate}}^{occ}$) and the OE exhibit lower amplitudes at low frequencies, while in the high-frequency range, they demonstrate higher amplitudes. The simulations generated by the modified virtual tester generally align with observed trends but notably underestimate $H_{p,acc_{plate}}^{occ}$ and OE across most of the frequency range of interest. The differences between measurements and simulations (mainly around 300 Hz and 800 Hz) can be attributed to the modal behavior of the ATF, which is exacerbated when the ear is compressed. An additional outcome of the important modal behavior of the test bench is a notable rise in measurement variability, particularly noticeable in the occluded configuration. The decision to adjust ear compression at $\pm 0.8\%$ during various measurements, as previously indicated, further amplifies measurement variability. This adjustment accentuates the ATF's responsiveness to ear compression, particularly at resonant frequencies. The increase in low-frequency variability ($f < 400$ Hz) is also explained by the lower quality of the transfer function measurement (coherence below 0.8). Indeed, compressing the ear results in the stiffening of the excited system, as seen by the shaker. This shifts the resonance frequency of the electrodynamic actuator towards higher frequencies; the frequency from which the system can inject vibrational energy into the ear.

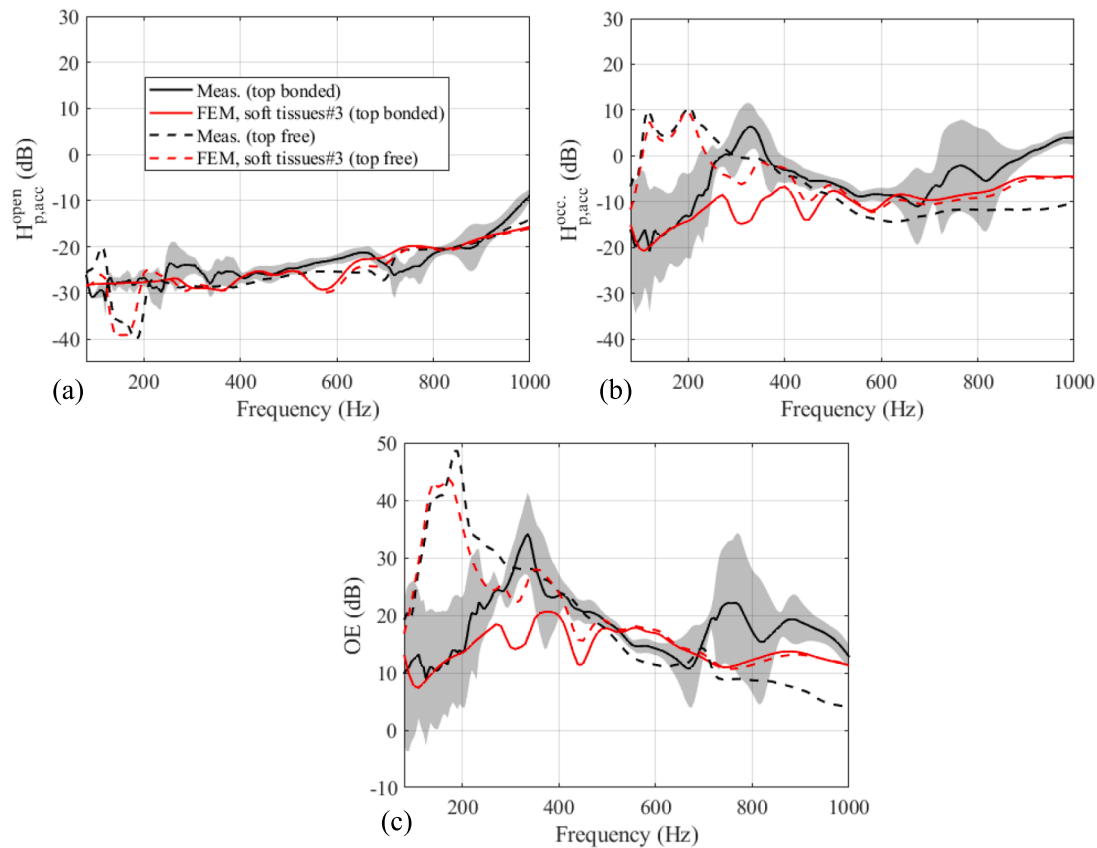


Fig. 13. Comparison between the simulation and measurement results in the case of the bonded boundary condition for the top side of the ear: transfer functions for (a) open ear, (b) occluded ear, and (c) objective OE. Simulation results based on the soft tissues set properties #3 are presented using the solid red curves; measurement results are presented using the thick solid black line. The experimental and numerical results of the original configuration (i.e., free boundary condition at the top side ear) are also presented in dashed black and red lines for comparison purposes.

All of the above findings justify the choice of leaving the ear free on the top in the current version of the proposed ATF. Indeed, this helps reduce the modal behavior of the test bench, which hinders the validation of the virtual tester (as the vibrational behavior of the bench is not modeled) and significantly increases measurement variability (since a precise control of the ear compression was not available on this ATF).

Appendix C. . Effect of the cartilage

Three distinct operations are conducted to examine the effect of the presence and positioning of the cartilage in the artificial ear (see Fig. 14). In Configuration 1, the cartilaginous component is entirely removed and replaced with soft tissues. For Configurations 2.1 and 2.2, the cartilage is vertically displaced by 1 mm and 1.5 mm, respectively. This adjustment brings the upper part of the cartilage closer to the ear canal cavity, while the lower part moves farther away. Configurations 3.1 and 3.2 involve systems in which the cartilage is rotated clockwise by 4° and 8° , respectively. By comparing the simulation results of these configurations, we can determine the potential OE difference resulting from the alteration in cartilage position. This sensitivity analysis on the impact of cartilage (presence and position) is conducted for two boundary conditions at the top side of the ear, namely, free and bonded.

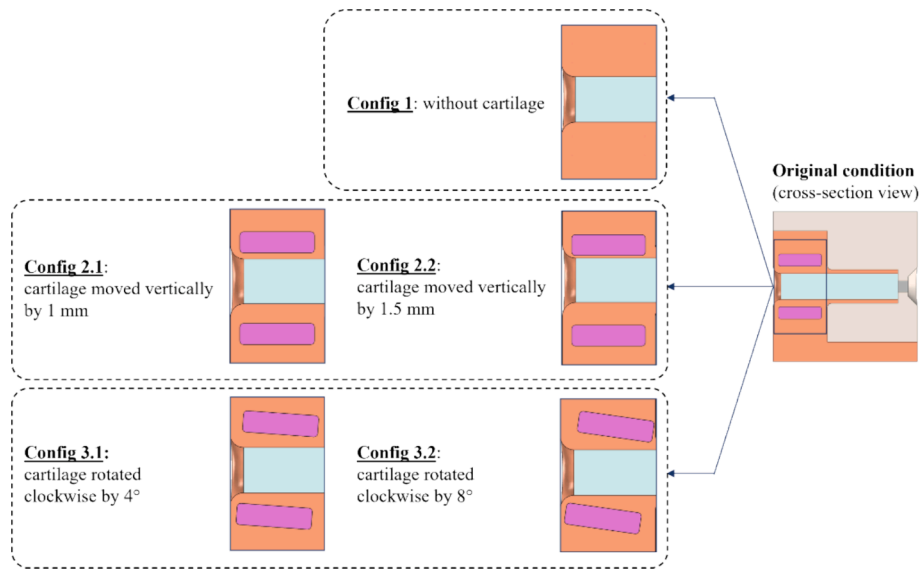


Fig. 14. Schematic representation of the numerical tests on the influence of the cartilage.

The simulation results corresponding to the five configurations in Fig. 14 are displayed respectively in Fig. 15. The results obtained with the model under original conditions are also provided for comparison (solid black curves). For the open ear, no distinguishable difference can be found from the simulated transfer function when changing the cartilage position. Differences within 3 – 4 dB are observed when the cartilage is completely replaced with the soft tissues. For the occluded ear, the presence or not of the cartilage has a very important influence on the transfer function in the whole frequency range of interest and this influence depends on the boundary condition. Compared with the original configuration, when the cartilage is replaced with the soft tissues, the overall stiffness of the coupled system is reduced. As a result, the volume velocity of the earcanal walls greatly increases (not shown here) and more sound energy is radiated into the earcanal cavity from its lateral walls. The OE (and the associated transfer functions) is not very sensitive to the position of the cartilage in the case of the “top free” boundary condition. In the case of the “top bonded” boundary conditions, the position of the cartilage may have an important influence up to 400 Hz. Moving vertically the cartilage position is found to increase greatly the transfer function at frequencies below 300 Hz, with the maximum increase of about 15 dB around 200 Hz. The closer the cartilage is positioned toward the earcanal cavity, the more pronounced the increase. However, rotating the cartilage does not greatly affect the transfer function, with only minor differences at frequencies below 200 Hz. As a result, removing completely the cartilage or moving it vertically, even by a small distance, would lead to evident changes in the OE in the corresponding frequency bands.

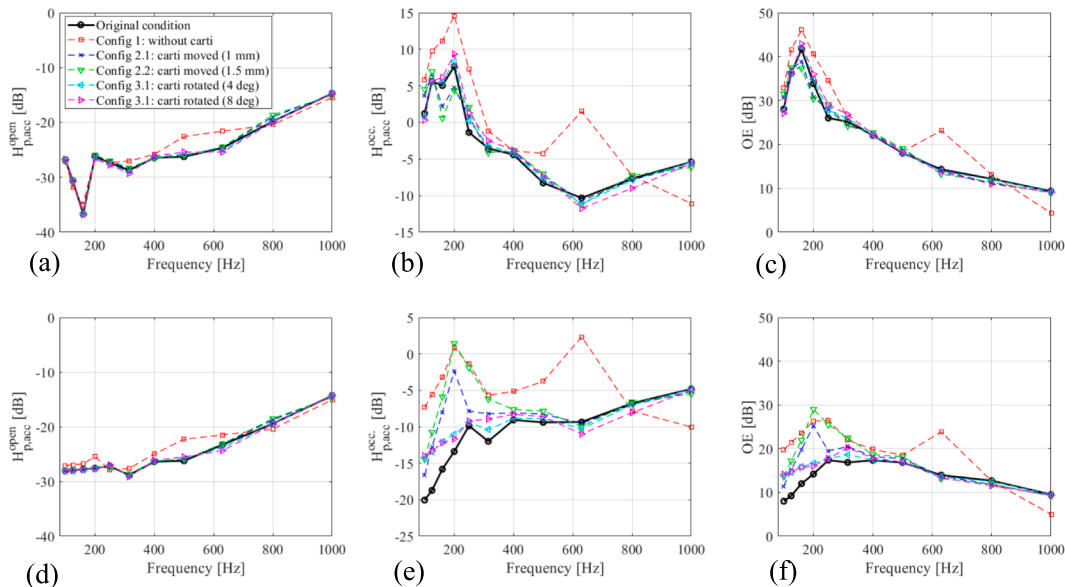


Fig. 15. Numerical test results on the influence of the cartilage for the two boundary conditions “top free” (first line) and “top bonded” (second line) and computed for the following three indicators: transfer functions for open ear ((a) and (d)), occluded ear ((b) and (e)), and objective OE ((c) and (f)).

This numerical study shows that the position of the cartilage in the outer ear has an influence only in the case of a compressed ear (condition of the ear being bonded at its top “bony” surface) at low frequencies ($f < 500$ Hz). If future research confirms that the position of the cartilage in the outer ear significantly influences the objective, subjective, and experienced OE in humans, impacting the design of in-ear devices, bonding the top side of the ear in the proposed ATF concept will become crucial for measurement realism. In that case, the test bench used to design the ATF, as well as the excitation system, should be improved to precisely control the artificial ear’s compression and avoid vibrational modes in the frequency band of interest.

References

- [1] Doutres O, Terroir J, Jolly C, Gauvin C, Martin L, Negrini A. Towards a Holistic Model Explaining Hearing Protection Device Use among Workers. *Int J Environ Res Public Health* 2022;19:5578. <https://doi.org/10.3390/ijerph19095578>.
- [2] Berger EH, Voix J. Hearing protection devices (chapter 11). In: Meinke DK, Berger EH, Neitzel RL, Driscoll DP, Bright K, editors. *Noise Man. 6th edition*. Falls Church (VA): AIHA Press; 2022.
- [3] Berger EH, Kerivan JE. Influence of physiological noise and the occlusion effect on the measurement of real-ear attenuation at threshold. *J Acoust Soc Am* 1983;74: 81–94. <https://doi.org/10.1121/1.389621>.
- [4] Reinfeldt S, Stenfelt S, Håkansson B. Estimation of bone conduction skull transmission by hearing thresholds and ear-canal sound pressure. *Hear Res* 2013; 299:19–28. <https://doi.org/10.1016/j.heares.2013.01.023>.
- [5] Stenfelt S, Wild T, Hato N, Goode RL. Factors contributing to bone conduction: the outer ear. *J Acoust Soc Am* 2003;113:902–13.
- [6] Stenfelt S, Reinfeldt S. A model of the occlusion effect with bone-conducted stimulation. *Int J Audiol* 2007;46:595–608.
- [7] Carillo K, Doutres O, Sgard F. Theoretical investigation of the low frequency fundamental mechanism of the objective occlusion effect induced by bone-conducted stimulation. *J Acoust Soc Am* 2020;147:3476–89. <https://doi.org/10.1121/10.0001237>.
- [8] Carillo K, Sgard F, Dazel O, Doutres O. Reduction of the occlusion effect induced by earplugs using quasi perfect broadband absorption. *Sci Rep* 2022;12:15336. <https://doi.org/10.1038/s41598-022-19641-3>.
- [9] Carillo K, Sgard F, Dazel O, Doutres O. Passive earplug including Helmholtz resonators arranged in series to achieve broadband near zero occlusion effect at low frequencies. *J Acoust Soc Am* 2023;154:2099–111. <https://doi.org/10.1121/10.0021185>.
- [10] ANSI/ASA S12.42. Methods for the Measurement of Insertion Loss of Hearing Protection Devices in Continuous or Impulsive Noise Using Microphone-in-Real-Ear or Acoustic Test Fixture Procedures 2014.
- [11] Xu H, Sgard F, Wagnac E, de Guise J. Development of an entire human head finite element model based on in-vivo medical images for investigation of sound transmission. *Proc. 26th Int. Congr. Sound Vib. ICSV26, Montreal, QC, Canada: 2019, p. 7.*
- [12] Xu H, Sgard F, Carillo K, Wagnac É, de Guise J. Simulation of the objective occlusion effect induced by bone-conducted stimulation using a three-dimensional finite-element model of a human head. *J Acoust Soc Am* 2021;150:4018–30. <https://doi.org/10.1121/10.0007230>.
- [13] Xu H. A finite element model of a human head and a corresponding acoustic test fixture to assess the objective occlusion effect induced by earplugs under bone-conducted stimulation. Ph.D. thesis. École de technologie supérieure, 2022.
- [14] Brummund M. Study of the occlusion effect induced by an earplug: numerical modelling and experimental validation. Ph.D. thesis. École de Technologie Supérieure, 2014.
- [15] Brummund M, Sgard F, Petit Y, Laville F, Nélisse H. An axisymmetric finite element model to study the earplug contribution to the bone conduction occlusion effect. *Acta Acust United Acust* 2015;101:775–88. <https://doi.org/10.1121/1.4864484>.
- [16] Cyr-Desroches M-O. Development of a simplified and realistic artificial ear for quantifying the objective occlusion effect / Développement d'une oreille artificielle simplifiée et réaliste pour quantifier l'effet d'occlusion objectif (in French). Master's Thesis. École de Technologie Supérieure, 2021.
- [17] Carillo K, Sgard F, Xu H, Guilloteau A, Benacchio S, Poissenot-Arrigoni B, et al. On the modeling of the objective occlusion effect induced by earplugs: Recent advances, challenges and perspectives. *Spectrum* 2021;38:8.
- [18] Carillo K, Doutres O, Sgard F. Numerical investigation of the earplug contribution to the low-frequency objective occlusion effect induced by bone-conducted stimulation. *J Acoust Soc Am* 2021;150:2006–23. <https://doi.org/10.1121/10.0006209>.
- [19] Kersten S, Möhlmann C, Vorländer M. Finite element simulation of the ear canal wall vibrations. *Acoust. Week Can. AWC23, Montréal, Canada: 2023.*
- [20] Poissenot-Arrigoni B, Benacchio S, Sgard F, Doutres O. An artificial ear to assess objective indicators related to the acoustical comfort dimension of earplugs: validation of a vibro acoustic model for insertion loss and occlusion effect assessment. *Proc. 26th Int. Congr. Sound Vib. ICSV26, Montreal, QC, Canada: 2019, p. 8.*
- [21] Brummund M, Sgard F, Petit Y, Laville F, Boutin J. Implementation of a simplified, artificial external ear test fixture for measurement of the earplug induced auditory occlusion effect. *Proc. Meet. Acoust. ICA, vol. 19, ASA; 2013.*
- [22] Benacchio S, Doutres O, Le Troter A, Varoquaux A, Wagnac E, Callot V, et al. Estimation of the ear canal displacement field due to in-ear device insertion using a registration method on a human-like artificial ear. *Hear Res* 2018;365:16–27. <https://doi.org/10.1016/j.heares.2018.05.019>.
- [23] Luan Y, Cyr-Desroches MO, Carillo K, Doutres O, Sgard F. Development and evaluation of an artificial ear for quantifying the objective occlusion effect. *24th Int. Congr. Acoust. ICA, Gyeongju, Korea: 2022.*
- [24] Poissenot-Arrigoni B, Law CH, Sgard F, Doutres O. Earcanal anthropometry analysis for the design of realistic artificial ears. *J. Acoust. Soc. Am., vol. 148, Chicago, IL, USA: Acoustical Society of America; 2020, p. 2779–2779. doi: 10.1121/1.5147737.*
- [25] ISO 18437-5:2011. Mechanical vibration and shock — Characterization of the dynamic mechanical properties of visco-elastic materials — Part 5: Poisson ratio based on comparison between measurements and finite element analysis. 2011.
- [26] ASTM D412-16. Test Methods for Vulcanized Rubber and Thermoplastic Elastomers Tension 2021. doi: 10.1520/D0412-16R21.
- [27] Krpovic S, Dam-Johansen K, Skov AL. Importance of Mullins effect in commercial silicone elastomer formulations for soft robotics. *J Appl Polym Sci* 2021;138: 50380. <https://doi.org/10.1002/app.50380>.
- [28] ASTM E132 – 17. Test Method for Poissons Ratio at Room Temperature 2017. doi: 10.1520/E0132-04R10.
- [29] Saint-Gaudens H, Nélisse H, Sgard F, Doutres O. Towards a practical methodology for assessment of the objective occlusion effect induced by earplugs. *J Acoust Soc Am* 2022;151:4086–100. <https://doi.org/10.1121/10.0011696>.
- [30] Blockwise Engineering. Model RSS Manual Crimper. *Blockwise Eng* 2023. <http://blockwise.com/low-cost-crimpers/model-rss/> (accessed November 20, 2023).
- [31] Dalaq AS, Melo LGC, Sgard F, Doutres O, Wagnac E. Pressure induced by roll-down foam-earplugs on earcanal. *Int J Mech Sci* 2023;241:107970. <https://doi.org/10.1016/j.ijmecsci.2022.107970>.
- [32] Luan Y, Sgard F, Nélisse H, Doutres O. A finite element model to predict the double hearing protector effect on an in-house acoustic test fixture. *J Acoust Soc Am* 2022; 151:3476–89. <https://doi.org/10.1121/10.0009835>.
- [33] Benacchio S, Doutres O, Wagnac E, Sgard F. Conception d'oreilles artificielles réalistes dédiées à l'étude du confort acoustique et physique des protecteurs auditifs intra-auriculaires. IRSST: Institut de recherche Robert-Sauvé en santé et en sécurité du travail; 2020.
- [34] ANSI/ASA S1.11-2004 (R2009). Octave-Band and Fractional-Octave-Band Analog and Digital Filters 2009.